Wave-pinning and cell polarity from a bistable reaction-diffusion system

Yoichiro Mori[2], Alexandra Jilkine[2], and Leah Edelstein-Keshet[1][2]

[1]Corresponding author. [2]Institute of Applied Mathematics and Department of Mathematics University of British Columbia, Vancouver, B.C. Canada V6T 1Z2, E-mail:mori@math.ubc.ca, jilkine@math.ubc.ca, keshet@math.ubc.ca

Abstract

Motile eukaryotic cells polarize in response to external signals. Numerous mechanisms have been suggested to account for this symmetry breaking and for the ensuing robust polarization. Implicated in this process are various proteins that are recruited to the plasma membrane and seggregate at an emergent front or back of the polarizing cell. Among these are PI3K, PTEN, and members of the Rho family GTPases such as Cdc42, Rac, and Rho. Many such proteins, including the Rho GTPases cycle between active membrane-bound forms and inactive cytosolic forms. In previous work, we have shown that this property, together with appropriate crosstalk endows a biochemical "circuit" (Cdc42, Rac, and Rho) with the property of *inherent* polarizability. Here we show that this property is present in an even simpler system comprised of a single active/inactive protein pair with positive feedback to its own activation. The simplicity of this minimal system also allows us to explain the mechanism using insights from mathematical analysis. The basic idea resides in a well-known property of reaction-diffusion (RD) systems with bistable kinetics, namely, propagation of fronts. However, it crucially depends on exchange between active and inactive forms of the chemicals with unequal rates of diffusion, and overall conservation to pin the waves into a stable polar distribution. We refer to these dynamics as *wave-pinning* and we show that this phenomenon is distinct from Turing-instability generated pattern formation that occurs in RD systems that appear to be very similar. We explain the mathematical basis of the phenomenon, relate it to spatial segregation of Rho GTPases, and show how it can account for spatial amplification, maintainance of polarity, as well as sensitivity to new stimuli typical in polarization of eukaryotic cells.

Key words: cell polarization; Rho GTPases ; bistable reaction-diffusion; stationary front

1 Introduction

Polarization and reorganization of the cytoskeleton, a fundamental attribute of eukaryotic cells, is essential for cell locomotion, morphogenesis, and division. The puzzle of what cellular machinery endows the cell with an ability to polarize has been a subject of great interest, both theoretically (1–5), and experimentally (6, 7). In many cell types, biochemical reorganization precedes a cytoskeletal and morphological response (8–11). Key players in this biochemical redistribution include the Rho family GTPases (12, 13) and other proteins that cycle between the cell membrane and the cytosol. In this paper, we explain what properties of such proteins could result in an inherent capacity for polarization.

We first list features of cell polarization to be explained. When an unpolarized cell is subjected to a transient stimulus in the form of a shallow chemical gradient or a highly localized signal on the cell periphery, it responds by reorganizing into two well-defined regions, front and back. We term this *spatial amplification*. In most cases, this polarized state is maintained even after the transient stimulus is removed (*maintenance*). Another hallmark of cell polarization is its *sensitivity* to new incoming signals. If a polarized cell receives a sufficiently strong secondary stimulus, it adjusts its polarization accordingly (For example, reversal of orientation is seen in neutrophils when the stimulus gradient is reversed (14)). Theories for cell polarization should account for all these behaviours. At the same time, our model is not meant to describe all features of chemotactic cells. Some cell types continually send out pseudopods even in the absence of stimulation (15, 16), a behaviour represented by other models (2), but not by ours. The fact that chemical polarization occurs even in actin-poisoned "round" cells (treated with the drug latrunculin) (17) suggests that the formation of random pseudopods can be decoupled from the polarity-generating mechanism (7, 18), and here is where our model resides.

We (19, 20) and others (21) have previously used reaction diffusion equations with a few key characteristics to model Rho GTPase dynamics and spatial redistribution. We showed that the inherent ability to robustly polarize a cell depends on the cycling between active, membrane-bound and inactive cytosolic forms of these proteins. In our models, a transient and localized stimulus to the system was spatially amplified to result in a robust subdivision of the cell into two clearly defined regions, front and back, where the concentration of the active forms are high and low, respectively. In our previous work (19, 20), specific crosstalk based on (22) was assumed between the three Rho GTPases, Cdc42, Rac, and Rho (See also related ideas in (21, 23)). We showed that the model system exhibits both maintenance and sensitivity. However, as in (21), but with a notably distinct mechanism, we here show that the essential features of polarity can be studied in a far simpler system, consisting of a single active-inactive pair of proteins. Studying a simplified system is important for several reasons. Since it is amenable to full mathematical analysis, we can understand how the mechanism works in detail. Such a study also helps to uncover essential features common to disparate GTPase networks found in distinct cell types.[1]

All the behaviours described above can be explained in the context of a specific property of a reaction diffusion system that we term *wave-pinning* (WP), namely, the evolution of a decelerating front that becomes stationary after transient behaviour. This mechanism differs from those based on local excitation and global inhibition (LEGI) models, or diffusive instability of the Turing type (2, 21, 24–27) in ways that will be specified below. We explain how wave-pinning occurs, and reveal its fundamental properties which are interesting from both a biophysical and a mathematical perspective.

---

[1] We could even speculate that such elementary biochemistry could have endowed polarizability to early "protocells" before signal transduction pathways had evolved to their current level of complexity.

1.1 Properties of Rho GTPases

We highlight the wave-pinning mechanism in the context of the known Rho-GTPase biochemistry, although other proteins could be candidates for similar wave-based phenomena (28, 29).

The Rho GTPase family, whose best studied members are Cdc42, Rac, and Rho, is conserved from amoeba to mammalian cells. These three members play a central role in cell motility (30, 31), yeast budding (13), cytokinesis and wound healing (32). Each Rho GTPase cycles between the plasma membrane (active GTP-bound form) and cytosol (inactive GDP-bound form, Figure 1(a)) with conversions facilitated by GAPs, GEFs, and GDIs (33). Rates of transition (34), relative rates of diffusion (35), and concentrations typical of rest and polarized states (36) are known.

Spatial zones of Rho GTPase activity are important for cell polarization (32). In yeast, active Cdc42 localizes to a single zone on the plasma membrane marking the bud assembly site. In echinoderms, a zone of active Rho determines the site of cleavage-furrow formation during cytokinesis (37). In neutrophils and other motile cells, Cdc42 and Rac have been associated with putative cell front, and Rho with the cell back (but see (38), and note that details likely differ between cell types). A comparison between neutrophils and *Dictyostelium discoideum*, for example, reveals that Cdc42 and Rho are missing in the latter. (RacB could be playing a role similar to Cdc42 (39).) These differences make it even more significant that in some cell types or conditions, a single Rho GTPase can act as a basic polarizing unit.

Experimental evidence suggests that Rho GTPase cycling is directly responsible for the polarization response. In yeast, for example, the accumulation of Cdc42 at sites of polarized growth depends crucially on a gene that codes for a single Cdc42 GEF (13). We and others (19–21) have hypothesized that exchange between membrane and cytosolic forms plays a practical role in generating robust cell polarity, and in this paper, we explain how this mechanism could work at the level of each individual Rho-protein.

1.2 Mathematical Modeling

Mathematical models of cell polarization and gradient sensing date back to work by Meinhardt and Gierer in the 1970's (1). Recent models based on known biochemistry include (3, 19–21, 23, 40–43), and are reviewed in (44–46). Theoretical capability models include (2, 25, 26, 47). Most models for polarization belong to a class of phenomena based on local self-enhancement and long range antagonistic reaction (48). Indeed, such a class contains a rich diversity of pattern-forming systems (mechanochemical (49), neuronal activation-inhibition (50), activator-inhibitor, and substrate-depletion reaction-diffusion). Mathematicians and physicists recognize distinct subclasses with unique, well-defined properties (51). The dynamics, bifurcation structure, and consequently their physical properties (robustness, sensitivity, speed) differ dramatically. Many pattern-forming reaction-difusion systems belong to the class of Turing. We show that ours does not, and that this has important biological consequences.

Previous work by our group in which changes in cell shape, crosstalk between Rho proteins and their effect on the cytoskeleton were considered (19, 20), addressed polarization in a more complex, and less analytically tractable framework. In the model study to follow, we explain the inherent ability to polarize in a simpler system.

As in (19, 20) we base our model on the membrane-cytosol cycling of Rho proteins, and further as in (21), we focus on the case of a single active-inactive pair. Bistability is an essential ingredient in our model and we first outline how this could be achieved in a biochemically reasonable way.

1.2.1 The well-mixed system

Consider, first, a well-mixed system consisting of an active form, A, and an inactive form, B, of the signaling protein with interconversion:

$$B \underset{k_{ab}}{\overset{k_{ba}}{\rightleftarrows}} A, \tag{1}$$

See Figure 1. The concentrations of these chemicals a, b would satisfy kinetics of the form

$$\begin{aligned} \frac{da}{dt} &= \text{Rate of activation} - \text{Rate of inactivation,} \\ &= k_{ba}\, b - k_{ab}\, a, \\ &\equiv f(a, b) \end{aligned} \tag{2}$$

where k_{ba}, k_{ab} are rate constants (units of $1/t$) and where we have defined the function $f(a, b)$ above. If only this exchange takes place, and no new material is produced or destroyed, then conservation in the well-mixed system implies that

$$\frac{db}{dt} = -\frac{da}{dt}.$$

We will refer to $k_{ba}\, b$ as the rate of activation, $k_{ab}\, a$ as the rate of inactivation, and $f(a, b)$ as the reaction kinetics (or as the reaction terms). Bistability necessitates that either one or both of k_{ba}, k_{ab} be nonlinear. Here we have chosen one of the simplest assumptions (among other possible variants), namely that there is cooperative positive feedback from the activated form onto its own production (via GEFs), whereas the reverse conversion (mediated by GAPs) takes place at constant basal rate, δ. Expressions for the rate constants consistent with these assumptions are

$$k_{ba} = k_0 + \frac{\gamma a^2}{K^2 + a^2}, \quad k_{ab} = \delta,$$

where k_0 is a basal GEF conversion rate, and positive feedback is represented by a Hill function with maximal rate γ and saturation parameter K. The Hill coefficient $n = 2$ is needed to achieve bistability. The resulting kinetic function

$$f(a, b) = b\left(k_0 + \frac{\gamma a^2}{K^2 + a^2}\right) - \delta a, \tag{3}$$

has the essential properties we need, and similar kinetics have been used in (52, 53), and in a number of superficially similar models based on Turing pattern formation. (See later detailed comparison of these distinct mechanisms). However, to a large extent, the details of this choice for the kinetic function $f(a, b)$ are arbitrary; only the qualitative aspects of the reaction term, and in particular, its bistability are critical. The well-mixed system has steady states when $f(a, b) = 0$, i.e., when

$$b\left(k_0 + \frac{\gamma a^2}{K^2 + a^2}\right) = \delta a. \tag{4}$$

For a fixed value of b, the corresponding values of a at these steady states can be visualized as intersections of a sigmoidal curve (LHS of Eq. 4) with a straight line of slope δ (RHS of Eq. 4). Up to three such intersections can occur, $a_-(b), a_T(b)$, and $a_+(b)$, the outer two of which are stable. (We label the steady states in increasing order, so that $a_- < a_T < a_+$.) The existence of at least two stable values of the activated form of the protein, a, is strongly suggested by experimental

observations: these would correspond to the values of a at the front and at the back of polarized cells. For the wave-pinning mechanism to work, we will require that there is some range of values of b ($b_{\min} < b < b_{\max}$) for which the above three steady states exist. More generally, any kinetic function $f(a, b)$ that admits such steady states in a range of values of b would be suitable for our mechanism to work.

1.2.2 The spatially distributed system

We now consider a one space dimension (1D) version of a reaction-diffusion system based on the bistable kinetics described above. We model the diffusion and exchange of the active forms (bound to the cell membrane), and the inactive forms (e.g., RhoGDP in complex with GDI's in the cytosol) along a cell diameter transect, front to back, approximated as a one-dimensional segment ($0 \leq x \leq L$; see Fig. 1(b)). We let a,b be concentrations of the active and inactive forms of the proteins, respectively, in units of molecules/length. Then

$$\frac{\partial a}{\partial t} = D_a \frac{\partial^2 a}{\partial x^2} + f(a, b), \tag{5a}$$

$$\frac{\partial b}{\partial t} = D_b \frac{\partial^2 b}{\partial x^2} - f(a, b). \tag{5b}$$

The rate of diffusion of the membrane-bound (active) form is known to be significantly smaller than its inactive cytosolic counterpart (35), so that $D_a \ll D_b$. We assume no flux at the ends of the domain, so that

$$\left.\frac{\partial a}{\partial x}\right|_{x=0,L} = 0, \quad \left.\frac{\partial b}{\partial x}\right|_{x=0,L} = 0. \tag{6}$$

In our case, a polar pattern would be a chemical distribution that is highest at one end of the cell, and decreases to its lowest value at the opposite end of the cell. Note that in some other models for cell polarization, the domain considered is the membranous perimeter of a cell, for which periodic boundary conditions are appropriate. In some of those cases, the interior of the cell is considered to be spatially uniform, and/or the fast-diffusing component is represented by its spatial average. Together, Eqs. 5 and 6 imply **mass conservation** in the spatially distributed system, i.e.

$$\int_0^L (a + b)\, dx = C. \tag{7}$$

The form of Eqs. 5 and the conservation, Eq. 7, make our model superficially similar to one proposed by (21). The depletion of b in production of a resembles the Gierer-Meinhardt substrate-depletion mechanism (24), and the saturation terms look much like terms used in more recent Meinhardt models (52) that we compare further on. However, it is well-known that the behaviour of an RD system is intimately connected to precise details of the reaction terms. For example, the reaction kinetics assumed by the authors of (21, 24, 52) do not satisfy the properties required for wave-pinning (Section 3), and our system does not admit a Turing diffusion-driven instability as does theirs. To check this, observe that in linearization of Eqs. 5 about the homogeneous stable steady states $a = a_-, a_+$, we obtain coefficients $c_{11} \equiv f_a(a, b) < 0$, $c_{22} \equiv -f_b(a, b) < 0$ that fail satisfy a necessary condition for Turing instabilities, namely $c_{11}/D_a + c_{22}/D_b > 0$.

1.2.3 Input stimuli

An external stimulus is known to increase activation of proteins such as Rho GTPases by upregulating the GEFs that convert inactive forms to active forms. Depending on the nature of the

stimulus, this increased rate of activation could be space and time dependent. To model the external stimulus, we superimpose an additional transient spatial stimulus-dependent activation function f_S (added to Eq. 5a and subtracted from Eq. 5b).

$$f_S(b) = k_S(x,t)b. \tag{8}$$

$k_S(x,t)$, the increased rate of conversion of B to A due to an external signal has some spatiotemporal dependence. The specific forms of k_S we used in simulations are listed in the Appendix.

1.2.4 Parameter values

For computations, we set parameter values as follows: We take cell diameter to be $L = 10\,\mu\text{m}$, and diffusion coefficients in the membrane ($D_a = 0.1\,\mu\text{m}^2\text{s}^{-1}$) and in cytosol ($D_b = 10\,\mu\text{m}^2\text{s}^{-1}$) as in (35). Similar values have been measured for membrane-bound Cdc42 in yeast (54). The average membrane lifetime of an activated Rac molecule is $2\,\text{s}$ (55), while GAP-stimulated GTP hydrolysis of Rho has been measured as $1.5\,\text{s}^{-1}$ (34). We thus let the inactivation rate be $\delta = 1\,\text{s}^{-1}$. GAP hydrolysis must be matched in magnitude by GEF activation. We thus take $\gamma = 1\,\text{s}^{-1}$. For the baseline GEF activity we take $k_0 = 0.067\,\text{s}^{-1}$. The parameter K has units of concentration of A. We normalize concentrations so that $K = 1$ (units of length^{-1}).

2 Results

We first discuss numerical results and then explain the basis of the phenomenon.

2.1 Polarization and Wave-pinning

We first demonstrate that the above model reproduces two salient features of cell polarization, *amplification* and *maintenance*, as outlined in the Introduction. In the numerical experiments described here, we start with the same total amount of material in the domain. We start with an unpolarized cell in which a is uniformly equal to its lower steady state value a_- corresponding to the spatially uniform value of b. We subject this cell to two types of transient stimuli, localized (k_S^{loc}) and graded (k_S^{grad}), as detailed in the Appendix. From the computational results (Figure 2(a,b)), we see that both external stimuli k_S^{loc} and k_S^{grad} result in a local increase in the active form a near the cell edge at $x = 0$. This local rise is spatially *amplified* by a sharp front of the active form that propagates into the cell. When this propagation eventually halts, a phenomenon we call *wave-pinning*, the pinned front represents a clear segregation of the cell into front and back. This polarized state is *maintained* indefinitely, even after $k_S = 0$. The final steady state solution is identical for both k_S^{loc} and k_S^{grad}.

We next ask whether our model cell exhibits *sensitivity* to new incoming signals, and whether it can reverse its polarity. In our 1D simulation, we study this as a response to a sequence of two stimuli of the form $k_S^{\text{grad}}(x,t)$ one following another, but with reversed polarity. (Fig. 2(c)): we first give the cell an initial graded stimulus, and then we reverse the gradient of the stimulus. The model cell at first polarizes in the direction of the initial stimulus. After the second stimulus, the cell repolarizes in the opposite direction after some hesitation.

In simulations with various stimuli of larger slope or magnitude (not shown), the response of the cell remains the same. After some transients, the level of the active form of protein, and the location of the sharp front dividing front from back is the same (as in Fig. 2a-c). This feature of the model is explained in our analysis and provides one prediction that distinguishes this from alternative mechanisms for polarity.

6

We model spontaneous cell polarization by starting with random initial data and no signal

$$a(x,0) = a_-(b_0) \cdot 2R, \quad b(x,0) = b_0,$$

where $0 < R < 1$ is a uniformly distributed random variable. Depending on the initial data, the cell can polarize in either direction (Figure 2(d)). In some runs we also observed solutions with persistent multiple peaks (not shown). Such multiple peaks also occur if the cell simultaneously receives two localized stimuli at its opposite ends (not shown), as in "two pipette" experiments (7, 56). In this case, waves enter the domain from opposing directions and appear to set up two opposing "fronts" at the two ends and a "rear" in the middle of the cell. We believe that such multiple peak solutions are metastable and eventually coalesce to form a right or left polarized state. (See Discussion).

2.2 Mathematical Basis of Wave-pinning

Our task, below, is to explain the phenomenon of wave-pinning on which amplification and maintenance of cell polarization are based. The informal arguments here are supported by matched asymptotic analysis, the details of which will be presented elsewhere.

Wave-pinning is made possible by three qualitative features of our model equations. The first of these features is **mass conservation** resulting from the interconversion kinetics and no-flux boundary conditions as given by Eqs. 5 and 7. The total amount of protein, $C > 0$ is constant even when an external signal is applied, $(k_S \neq 0)$ since such signals simply increase the rate of conversion from B to A without affecting the combined total amount of A and B in the domain.

The second feature is spatial uniformity of b (to first approximation) that results from the assumption $D_a \ll D_b$; b quickly diffuses to attain a uniform value within the domain on the time scale of interest. This amounts to replacing Eq. 5b by the average value of b, a reduction often used in other models (2). This implies that the inactive form, Rho-GDP acts as a **global variable**. The third feature is **bistability** of the reaction term, i.e. the fact that, for b fixed in some range $(b_{\min} < b < b_{\max})$, the equation $\partial a/\partial t = f(a,b)$ admits steady states $a_- < a_T < a_+$ where a_-, a_+ are stable. We also require that the homogeneous state $(a,b) \equiv (a_\pm(b), b)$ be a stable stationary state of the reaction diffusion system.

We shall see below that the wave-pinning mechanism is dependent on wave-propagation, and is thus distinct from a Turing mechanims, which is based on growth of small local perturbations. One manifestation of the difference of the two models is that wave-pinning can act much faster to generate a polar pattern than does a related Turing-type mechanism, and this has important biological implications (see the section A comparison of models for details).

2.2.1 The single variable case (fixed b)

First, to develop the context, consider what happens in a single one-dimensional reaction diffusion equation for a on $0 < x < L$, with the above bistability property, and with b taken as parameter:

$$\frac{\partial a}{\partial t} = D_a \frac{\partial^2 a}{\partial x^2} + f(a,b). \tag{9}$$

On an infinite domain, Eq. 9 is known to possess a propagating front solution (49, 57). At the rear (respectively, front) of the wave ($x \to \pm\infty$) the profile asymptotes to a_+ (respectively, a_-). Suppose a, obeying Eq. 9 on $0 < x < L$, develops a propagating front that is sufficiently sharp and far from boundaries; then we can approximate its region of validity by $-\infty < x < \infty$. Let

$$a_f(\xi) = a_f(x - ct) = a(x,t).$$

Then it is known (49, 57) that the speed of the front, c, which need not be constant, satisfies

$$c(b) = \frac{\int_{a_-}^{a_+} f(a,b)da}{\int_{-\infty}^{\infty} (\partial a_f(\xi)/\partial\xi)^2 \, d\xi}. \tag{10}$$

c depends on b through its dependence on $a_-, a_+, f(a,b)$ and a_f. The denominator of Eq. 10 is positive, so the sign of $c(b)$ depends only on the integral in the numerator, which we denote hereafter by $I(b)$. For the reaction term in Eq. 3, the quantity $I(b)$ can represented geometrically by (signed[2]) areas between the sigmoidal curve for activation ($y = bk_{ba}$) and the straight line for inactivation ($y = ak_{ab}$) considered as functions of a, shown on the right panels in Figure 3. For example, in the top right panel of Fig. 3, there are two regions between these intersecting curves (shown in different shades), one clearly having an area of greater magnitude than the other. For our reaction term, there is one critical value $b = b_c$, (in $b_{\min} < b_c < b_{\max}$) at which the areas described above are equal and opposite (bottom right panel, Fig. 3). At this value of b, the speed $c(b)$ changes sign. If $b < b_c$, c is negative and if $b > b_c$, c is positive. The speed is zero when the following condition is satisfied[3]:

$$I(b) \equiv \int_{a_-}^{a_+} f(a,b)da = 0. \tag{11}$$

The two important properties we use below are: (1) there are two stable steady states for $b_{\min} < b < b_{\max}$, and (2) the integral $I(b)$ changes sign at $b = b_c$ (with $I(b) > 0$ for $b > b_c$).

2.2.2 Wave-pinning in the full a, b system:

The explanation of wave-pinning now proceeds solely on these premises. Suppose that initially a is at its basal steady state level and b is sufficiently high ($a(x,0) = a_-(b), b(x,0) \approx$ constant $> b_c$) (Figure 3). A transient stimulus near the edge of the cell at $x = 0$ triggers a local increase to the level $a \approx a_+$, via bistability. According to Eq. 10, and using the fact that $b(0) > b_c$, this creates a front that starts to propagate in the positive direction, converting a greater fraction of the domain to $a \approx a_+(b)$. By Eq. 7, as the amount of a increases, b must simultaneously decrease, eventually reaching the critical value $b = b_c$ at which wave-pinning occurs (left panels, Figure 3). The depletion of b to its critical level b_c causes the wave to pin.

2.2.3 Tracking the evolving front:

Using the fact that the wave stalls at $b = b_c$, we can compute the position of the front of the pinned wave, hereby denoted x_p. For a sharp front, $a \approx a_+$ to the left (respectively a_- to the right) of x_p. (The values of a_-, a_+ are obtained from the steady state equation $f(a, b_c) = 0$.) Conservation of the total, C from Eq. 7, and spatial uniformity of b, imply that, to first order,

$$a_+(b_c)x_p + a_-(b_c)(L - x_p) + b_c L = C. \tag{12}$$

The front position, x_p, is obtained by solving Eq. 12. Numerical computations give excellent agreement with this prediction.

Because the position of the front is defined by Eq. 12, only the parameters in the model (rate constants in Eq. 3) that determine the steady states, domain size L, and total amount of protein C influence the polar state. This means that *transient* gradients or localized stimuli lead to the same

---

[2]The sign of the area is positive where activation is greater and negative where inactivation is greater.
[3]In some sources this is called a *Maxwell condition* (27, 58))

level of active protein at the front, and the same position of the front, explaining the similarity of results in Fig. 2(a-c) and other simulations with a variety of gradient magnitudes.

From the above argument, it is evident that wave-pinning would *not* occur if there is initially too little inactive form, e.g., $b < b_c$ at $t = 0$. Even if there is enough, i.e. if $b > b_c$, wave-pinning would fail if the reduction in b as the front sweeps through the domain is insufficient to reach the level $b = b_c$ inside the given domain. If initially b is too high, or if the cell is too small, wave-pinning will also fail because Condition 12 cannot be attained. For fixed domain size L, the possibility of wave-pinning is determined by the total amount, C, of a and b. Our analysis predicts that the size of the activated region (i.e. portion of the domain for which a is at its high steady state value) will be an increasing function of C.

To obtain a better understanding of wave-pinning, we consider a caricature of the reaction term that is simple enough to be fully analytically tractable while encompassing all required qualitative properties. We let

$$f^{\text{cubic}}(a, b) = -k(a - a_-(b))(a - a_{\text{T}}(b))(a - a_+(b)), \tag{13}$$

$$\text{where } a_- = \ell b, \quad a_{\text{T}} = h, \quad a_+ = mb, \quad a_- < a_{\text{T}} < a_+. \tag{14}$$

with $m < \ell$. Here, the straightforward dependence of steady states on the level of b makes the analysis go through. Using Eq. 12 and simple algebra, it can be shown that the front will stall inside the domain (i.e. that $0 < x_p < L$) provided

$$\frac{2h}{\ell + m}(1 + \ell)L < C < \frac{2h}{\ell + m}(1 + m)L. \tag{15}$$

Constant homogeneous solutions also exist provided

$$C = b(\ell + 1)L < \frac{h(\ell + 1)L}{\ell}. \tag{16}$$

It is straightforward to show that the constant homogeneous solutions with $a(x) = a_-$ or $a(x) = a_+$ are stable as solutions of the full RD system, Eqs. 5,13. Furthermore, this system does *not* admit a Turing diffusive instability for functions f satisfying the minimal conditions for wave-pinning, in contrast with the reaction terms assumed by (21). For a given set of values m, ℓ, h it is possible to find a range of values of C that satisfy both conditions 15 and 16. This implies coexistence of *both* unpolarized and polarized states over the *same* range of parameters. The system would then asymptotically approach either one or the other configuration depending on initial conditions and on the applied transient stimulus f_S. This behavior is seen in simulations with the biochemically motivated reaction term in Eq. 3, e.g., in Supplementary Fig. 3.

In general, and specifically for reaction terms of type 3, an explicit form for the propagating front solution $a_f(\xi)$ in the denominator of Eq. 10 is not obtainable. However, the simplicity of the cubic reaction kinetics in Eq. 13 allows us to evaluate the integrals in Eq. 10 explicitly as a function of b. Using matched asymptotic expansions (details to be presented elsewhere), we obtain a closed form ordinary differential equation (ODE) for the evolution of the front position $x_f(t)$:

$$\frac{dx_f}{dt} = \sqrt{2kD_a} \left(\frac{C(m + l)}{2((1 + \ell)L + (m - \ell)x_f)} - h \right). \tag{17}$$

We can thus reduce a system of two partial differential equation to a single ODE for the propagating front position. The front becomes stationary when $dx_f/dt = 0$, at

$$x_f = \frac{1}{(m - \ell)} \left(\frac{C(m + \ell)}{2h} - (1 + \ell)L \right). \tag{18}$$

9

In Figure 4, we plot the front position calculated by solving the partial differential equation and tracking its evolving front, as well as the position obtained by solving the above ODE directly. We see excellent agreement between the two curves.

3 A comparison of models

In this section, we discuss two competing models from the literature, the local excitation global inhibition (LEGI) model (18, 59), and the activator substrate-depletion model (ASDM) (1, 24, 60). Detailed comparisons of behaviour of these and our wave-pinning (WP) model are given in the Supplementary Information. Superficial similarities aside, the models are based on distinct nonlinear dynamics phenomena, and predict contrasting behaviours in response to a suite of external stimuli.

3.1 The Local Excitation Global Inhibition (LEGI) Model

The LEGI Model in its basic form (18, 59) is specifically designed to exhibit *adaptation* to spatially uniform stimuli. Its chemicals include two that are produced in direct proportion to an external stimulus $S(t, x)$; these are a membrane-bound (localized) activator, A, and a diffusible (global) inhibitor, I. A third, localized chemical R, creates the response. Generic LEGI models contain too few nonlinearities and spatial terms to have inherent pattern-forming or wave-propagating features of their own, and are not intended as such. Rather, LEGI models are ideal as a readout of persistent macroscopic signals of various amplitudes. LEGI modules are normally coupled to other hypothesized chemical circuits to amplify or shape aspects of the behaviour (18, 27, 45, 61). Typically the response of a LEGI model on its own includes a transient phase (elevation of A, I and R), followed by polarization (for a sustained gradient stimulus), or return to a rest state (for a homogeneous constant signal or for any transient signal after it is turned off).

Excellent reviews of the LEGI models, and their application singly, coupled to amplification models, and/or to one another appear in the literature (18, 45, 47, 59, 61), and details are here omitted for brevity. In Fig. 1 of the Supplementary Information, we demonstrate prototype responses to the same repertoire of stimuli used in our wave-pinning tests. Unlike the wave-pinning model, the LEGI model does not have a threshold for stimulation, does not have persistence memory of a stimulus, and does not polarize in response to spatially noisy perturbation of the homogeneous steady state. However, it does allow for reversal of polarity when the stimulus gradient is reversed. (See Supplementary Figs. 1, 3.)

3.2 The activator substrate-depletion model (ASDM)

Several variants of RD systems in which a substrate (b) is depleted in the production of an activator (a) are given in the literature. Some of these have been described decades ago (1, 24), and certain variants have been analyzed thoroughly for pattern-forming properties[4]. In general, related systems can exhibit other pattern-formation phenomena such as spots, stripes, labyrinthian patterns, peak-splitting or merging, etc. Substrate-depletion models that include saturation terms have been used in larger models for other biological phenomena[5](52). Cytoplasmic diffusion is sometimes replaced by averaging. For the purpose of comparison, we chose a two-variable saturating kinetics variant

---

[4]See, e.g. (49), where the name "Schnackenberg" is occasionally associated with essentially the same system. The "Brusselator" reaction (62) is related to these as well.

[5]An anonymous reviewer of this paper pointed out that saturation leads to a plateau distribution, with peaks that are more easily shiftable to favorable positions.

(kindly supplied by Prof. H. Meinhardt) whose various terms most closely resemble those of our own model,

$$\frac{\partial a}{\partial t} = b\left(\frac{sa^2}{1 + s_a a^2}\right) - r_a a + D_a \frac{\partial^2 a}{\partial x^2}, \tag{19a}$$

$$\frac{\partial b}{\partial t} = b_b - b\left(\frac{sa^2}{1 + s_a a^2}\right) - r_b b + D_b \frac{\partial^2 b}{\partial x^2}. \tag{19b}$$

As in our model, positive feedback from a to its own production is governed by a Hill function with an amplitude s and a saturation parameter s_a. This production of a in Eq. 19a is at the expense of b in Eq. 19b. It is assumed that the diffusion of the substrate is greater than the diffusion of the activator $(D_b > D_a)$. Such positive feedback with a *limited* substrate supply has been used in many chemotaxis models, but the striking similarity of Eqs. 19 to our Eqs. 5 with kinetics of Eq. 3 is misleading. Significantly, the system 19 does not satisfy a conservation principle such as Eq. 7 and consequently *cannot* admit a wave-pinning mechanism: the decay rates of the activator and substrate, (r_a, r_b) and constant input of substrate (b_b) are inconsistent with simple interconversion of a and b, and the total amount is not conserved.

Unlike our model, Eqs. 19 *do* admit a Turing (diffusion-driven) instability and this is the mechanism associated with the pattern forming ability of that model. We explain the implications of this fact in Section 3.3. In the Supplementary Information, we also describe how a comparison was made between the ASDM and WP model using the same repertoire of stimuli. Briefly, the evolution of a polar pattern is found to occur to arbitrarily small perturbations of the uniform steady state, but to evolve more slowly than wave-pinning (for reasons outlined below). ASDM polarity is locked, once formed, and does not on its own reverse if the stimulus gradient is reversed. (See Supplementary Figs. 2, 3.)

3.3 Time to polarize

Some estimates for the conditions for polarization and the temporal behaviour in the distinct models is obtainable from dimensional considerations, linear stability, and asymptotic analysis. Here, we concentrate on the specific case of diffusion coefficients relevant to Rho proteins $(D_a \ll D_b)$, for a context in which to compare the models. A comparison in full generality is beyond our scope, since the essential behaviour of the models is so different.

A preliminary remark is that any model based on Turing instability (such as ASDM) is associated with a dispersion relation that describes the growth rate $\sigma(q)$ of any wavenumber q. At the Turing bifurcation, a single critical wavenumber q_{crit} becomes unstable, and its corresponding growth rate $\sigma(q_{\text{crit}})$ just turns positive. A pattern of the form $\cos(q_{\text{crit}} x)$ then starts to grow. A tradeoff then exists between tuning parameters to increase the growth rate of this pattern, versus preventing other wavenumbers from also becoming unstable. If the importance of having a specific pattern (e.g. a polar one) is strong, then strict limitations occur on how rapidly that pattern can grow from a small perturbation.

Now consider the conditions for polarization in the WP and ASDM systems. Let representative reaction rate parameters be $\gamma_{\text{w}}, \gamma_{\text{s}}$ (units 1/time) in these mechanisms and L be the domain size. Then, in order for polarization to occur at all, the parameters must fall approximately within the

following ranges :

$$\sqrt{\frac{D_b}{\gamma_{\mathrm{w}}}} \sim L \qquad\qquad\qquad \text{Wave-pinning} \qquad\qquad (20)$$

$$\sqrt{\frac{D_a}{\gamma_{\mathrm{s}}}} \sim L \qquad\qquad\qquad \text{Substrate Depletion} \qquad\qquad (21)$$

(No such restriction exists in the LEGI model). The first condition is obtained from asymptotics and scaling in WP (the details of which will be presented elsewhere); the second is a condition for Turing instability in the case $D_a \ll D_b$.

Define chemical reaction times, $\tau_{\mathrm{w,s}}$, and times for diffusion of the substances, $\tau_{\mathrm{D}}^{a,b}$ by

$$\tau_{\mathrm{w}} = 1/\gamma_{\mathrm{w}}, \quad \tau_{\mathrm{s}} = 1/\gamma_{\mathrm{s}}, \quad \tau_{\mathrm{D}}^a = L^2/D_a, \quad \tau_{\mathrm{D}}^b = L^2/D_b.$$

Then, the above conditions can be rewritten as:

$$\tau_{\mathrm{D}}^b \sim \tau_{\mathrm{w}} \qquad\qquad\qquad \text{Wave-pinning} \qquad\qquad (22)$$
$$\tau_{\mathrm{D}}^a \sim \tau_{\mathrm{s}} \qquad\qquad\qquad \text{Substrate Depletion} \qquad\qquad (23)$$

In order to work, both mechanisms are predicated on a balance of a diffusion time scale with a reaction time scale, but note that the diffusive time scale in question are different in the two mechanisms since $\tau_{\mathrm{D}}^b \ll \tau_{\mathrm{D}}^a$. One implication here is that reaction rates must be rather slow, in keeping with the slow diffusion of the activator in ASDM, or else no polarization would be possible. By comparison, the reaction rates in WP could be much faster, as they must only balance the diffusion rate of the rapidly-diffusing inactive form.

Suppose now that the above conditions are satisfied. Then, the transition times $T_{\mathrm{w,s}}$ to the polarized state can be expressed approximately as follows:

$$T_{\mathrm{w}} \sim \frac{L}{\sqrt{\gamma_{\mathrm{w}} D_a}} = \sqrt{\tau_{\mathrm{w}} \tau_{\mathrm{D}}^a} \qquad\qquad \text{Wave-pinning} \qquad\qquad (24)$$

$$T_{\mathrm{s}} \sim \frac{1}{\gamma_{\mathrm{s}}} = \tau_{\mathrm{s}} \qquad\qquad\qquad \text{Substrate Depletion} \qquad\qquad (25)$$

The first of these is obtained from considerations of the speed of the wave that moves into the domain in the wave-pinning model. The second estimate is obtained from an approximation for the largest positive eigenvalue (growth rate of the most unstable mode), close to a Turing instability, in the case $D_a \ll D_b$.

Thus, in the wave-pinning mechanism, the diffusion coefficient of the inactive form dictates the possibility of the polarization response, whereas the diffusion coefficient of the active form determines the speed with which the polarized state is reached. In the substrate depletion model, the diffusion coefficient of the active form dictates the possibility of polarization whereas the speed of the polarization response is solely determined by the reaction rate. We describe a related timescale for LEGI polarization in the Appendix.

From Fig. 2a, we note yet another timescale of importance in the wave-pinning model, and that is the initial "jump" between the steady states a_- and a_+. This dynamic is responsible for creating the large difference in cell edges very rapidly in response to a stimulus applied at one edge. This time, T_{Resp} is also of the order

$$T_{\mathrm{Resp}} \sim \frac{1}{\gamma_{\mathrm{w}}} = \tau_{\mathrm{w}}, \qquad \text{Initial jump, Wave-pinning}$$

12

However, as noted above, in wave-pinning, a much faster reaction rate is consistent with polarization, and consequently this response time is also much faster, as discussed in the comparisons of Figs. 2 and Supplementary Fig. 2.

For example, for rates of diffusion $D_a = 0.1, D_b = 10 \, \mu m^2 s^{-1}$ typical of the active and inactive Rho GTPases, with cell size on the order of $L \approx 10\mu m$, we find the following: reaction times on the order of one to a few seconds that characterize Rho GTPases, would be consistent with a wave-pinning mechanism ($\tau_w \approx \tau_D^b \approx 1 - 10s$). However the substrate-depletion mechanism requires that reaction times be on the order of $\tau_s \approx \tau_D^a \approx 1000s$, likely too slow to be consistent with Rho GTPase kinetics.

Furthermore, if we compare the time to complete polarization in the two mechanisms, we find that $T_w \approx \sqrt{\tau_w \tau_D^a} \approx \sqrt{1 \cdot 1000} \approx 30s$ for wave pinning. By comparison, the time to polarization in the substrate depletion mechanism ($T_s \approx \tau_s$) would be on the order of some hundreds to thousand seconds (about 20 min), which is slower than seen experimentally. As mentioned above, the wave-pinning mechanism has an even faster response when we consider the fact that an initial jump already defines a clear polarity even before the final polarized state is attained. This occurs on a timescale of τ_w, i.e. within a few seconds. There is no comparable "fast" response in the substrate-depletion model. (Compare also Fig. 2 in the text with Fig. 3 in the Supplementary Material for simulations illustrating the same conclusions.) These rough estimates illustrate the distinctions between the mechanisms and suggest that the wave-pinning mechanism may be inherently better for polarizing a cell rapidly.

4   Discussion

In this paper, we have used simplification to reach a better understanding of phenomena that we previously observed in more detailed models containing a larger parameter set. By reducing those models to the minimal plausible scenario, we have explained how a single pair of proteins in active and inactive forms, cycling between plasma membrane and cytosol, together with conservation and cooperative positive feedback could suffice to provide a basic cellular polarization mechanism. Part of this analysis points to the functional importance of such membrane-cytosol exchange and its role in separating the rates of diffusion of the intermediates. Candidates for proteins that have such features are the Rho-GTPases with their GEF-mediated activation and GAP-mediated inactivation. Cytosolic Rho-GTPases, the inactive forms, diffuse up to two orders of magnitude faster than the active membrane-bound forms. Thus, the inactive forms inherently act as "global information carriers". Unlike some models for cell polarity with global or long-ranged inhibition, our model is based on a depletion mechanism, but one in which simple interconversion guarantees a conservation principle.

One of the contributions of our investigation is the proposal that not only pattern forming mechanisms, but also wave-propagation based aspects of reaction-diffusion systems, and specifically the freezing and pinning of those waves, can lead to cell polarity (See also (63) for a recent wave-based cell motility model.) A second contribution is the explicit formulation of the necessary qualitative properties that the reaction term $f(a, b)$ must satisfy for the wave-pinning mechanism to work. Given that reaction diffusion equations can exhibit a wide range of phenomena depending on the choice of reaction term, it is difficult to judge how general or applicable are behaviours of specific examples (such as those in (21)) without this type of qualitative characterization.

Our model captures a number of essential properties of cellular polarization. First, a "model cell" responds to a variety of stimuli by spatially amplifying the stimulus, and attaining a polarized state. This occurs for both localized as well as graded signals (Figs 2(a-b)). Second, the polarization

13

is maintained even after the signal is removed. Third, the cell remains sensitive to further stimuli, and reverses its polarity in response to a sufficiently strong second signal of opposite orientation (Figs 2(c)). Finally, the model cell polarizes in response to spatially random ("noisy") signals under some circumstances (Fig 2(d)). Such behavior characterizes the responses of numerous cell types, from *Dictyostelium discoideum* to neutrophils.

Several types of experimental findings lend support to application of this model to Rho GTPases. Some biochemical evidence of a positive feedback loop in Cdc42 activation (64) supports the Hill function term in our kinetics in Eq. 3. Other evidence points to phosphorylation of RhoGDI as a possible mechanism to control which proportion of Rho GTPase is in the active form (65, 66). In yeast, the cycling of Cdc42 between its GTP and GDP bound states is known to be crucial for polarization (67). Furthermore, other proteins signalling to Cdc42 such as Rsr1p (Bud1p) can exist in both membrane-bound and cytosolic fractions, and deletion of these proteins leads to a travelling patch of active Cdc42 rather than a stable cap formation (53).

The model suggests a number of experimental tests that could be used to check its validity. For example, we predict that incremental overexpression of the Rho protein in the cell would incrementally shift the position of the transition zone. Beyond some level, further overexpression should abolish cellular polarity altogether, as the total amount of protein in all forms no longer satisfies the condition required for wave-pinning inside the domain.

The basic polarity module described here (or variants with the same qualitative structure) could be embedded in larger pathway structures, with feedbacks that fine-tune, modulate, and adapt the response to the given cell type, conditions, and stimuli. Crosstalk of Rho GTPases (Cdc42, Rac, and Rho) occurs in neutrophils and other cell types (6, 68). These have been explored elsewhere and shown to give rise to spatial polarization and mutual exclusion between Cdc42/Rac and Rho both in one (20, 21) and two (19) spatial dimensions. Other pathways could account for stochasticity of the response, periodic formation of pseudopods, or a spatially uniform rise of signal and return to rest (*adaptation*) in response to a uniform signal observed in *Dictyostelium* (8). Additional pathways or crosstalk can also help to hone sensitivity to small gradients (17, 20) or to accelerate the resolution of multiple peak patterns into a single front (46).

Other models have been proposed to explain cell polarization and chemotactic gradient sensing, some of which we briefly compared in a previous section. Many models are based on a diffusive Turing-type instability or on local excitation global inhibition (LEGI) mechanisms (2, 25–27). The identity of the inhibitor is still controversial in such models. The work of (43) includes some models with depletion of components, but is otherwise directed towards other aims. Some models share similar elements with ours. For example, in (4), directional sensing also depends on a membrane-bound and a cytosolic species (e.g. α and $\beta-\gamma$ subunits of a heterotrimeric G protein), but these are not conserved: they are both produced at equal rates. A switch-like response to external gradients is also discussed. In (53), a similar behaviour is obtained in polar coordinates (i.e. along the perimeter of yeast cell), with related kinetic terms, but without characterization of the mechanism of wave-pinning. Our own previous work (19, 20) demonstrated the phenomenon of wave-pinning in systems of Rho GTPases, but the greater complexity of the six-PDE version discussed there (with crosstalk between Cdc42, Rac, and Rho) was much less transparent mathematically.

A recent model of (21) is probably the closest to our system in its overall formulation. The authors also identify Rho GTPases, and global conservation of active and inactive forms as important for cell polarization. Their model is also built on a system such as Eqs. 5, but notably, with different type of term for the reaction rate, $f(a, b)$. The authors used two specific reaction terms for which explicit computations could be carried out. Neither of these choices satisfy the conditions for bistability and wave-pining. Rather, the cell polarization mechanism proposed in (21) is based on a Turing-type diffusive instability. Their homogeneous state becomes unstable to

arbitrarily small perturbations, unlike our own system where conditions for Turing instability are not satisfied. In our hypothesis about the type of reaction term (given by Eq. 3, or 13, or other variants with similar qualitative properties), polarization results from front-propagating behavior of the bistable reaction diffusion system.

Unlike mechanisms based on a Turing instability, the homogeneous state is linearly stable (i.e., stable to very small perturbations) in our model. It requires a stimulus of finite, possibly small[6], amplitude to polarize the cell (Supplementary Fig. 3). We argue that this property is beneficial, as it allows for stability of a resting (unpolarized) cell to arbitrarily small noise. The difference in these mechanisms is reflected in the requirement on the diffusivities. In (21), the authors only require $D_a < D_b$ whereas we require that D_b be *much* larger than D_a, a requirement satisfied by Rho proteins. In comparing our model to two competing models, LEGI and ASDM, we have shown that predictions of these differ in numerous aspects. A single LEGI module is a graded readout of signal that does not remember a stimulus once it is removed, but this facilitates a sensitivity to new stimuli. The ASDM model can polarize in response to the smallest spatial noise but its generated pattern is subject to locking; also, the requirement of a polar pattern (rather than one with two or more activator peaks) can make its response inherently slower that of the wave-pinning mechanism. Both LEGI and ASDM models can produce a panoply of realistic behaviour when embedded in larger systems that modify or complement their basic behaviour (47, 52). Our model too, becomes more complex, capable of more subtle responses, and more realistic when embedded in a larger system that specifically describes Rho protein and phosphoinositide feedbacks (19, 20, 46).

The mechanism may prove to have greater implications in cell biology: any bistable kinetics, together with reduced mobility of one of two interchangeable states (e.g. due to binding to the cytoskeleton, membrane, or other cellular structures) could, in principle, lead to similar phenomena. It would be of interest to explore other pairs of interconvertible biochemical agents that share the characteristics here specified. (Par proteins and assymetric division in the *C. elegans* embryo may be one example; A. T. Dawes, personal communication.) Bistability in protein-kinase cascades has been noted as a mechanism for promoting waves that allow rapid long-range signalling across cells (see, e.g. (29)). Here we showed that bistability also leads to stable fronts, and subdivision of the cell into multiple domains.

Aside from application of our model to cell biology, several mathematical implications merit discussion. Many reaction-diffusion systems with bistable reaction terms admit travelling wave solutions (49). Waves can be stopped by specific parameter values consistent with a Maxwell condition (analogous to Eq. 11), but zero velocity fronts are generally structurally unstable, and do not persist if parameters in the model are perturbed slightly. In our coupled bistable RD equations, wave-pinning occurs within a *range* of parameter values. Within that parameter range, an appropriate input can lead to formation of a moving front that decelerates as it propagates, and that freezes at some predictable position; the location of that frozen front depends on parameters and on the total amount of material, i.e. on the initial configuration. We have also shown that such solutions coexist with stable spatially uniform steady states: the same range of parameter values is consistent with both uniform and stationary front asymptotic solutions. Similar RD systems on an infinite domain (69), or without conservation (70, 71) miss this phenomenon.

Our model is closely related to the globally constrained Allen Cahn equations consisting of one reaction diffusion equation with a global integral constraint (72–74). These equations are used to model phase separation, and support structurally stable zero velocity front solutions. Our wave-pinning argument above rested upon the reduction of our reaction diffusion *system* Eqs. 5 to a single equation where the equation for the inactive form $b(x)$ was reduced to an integral constraint. For

---

[6]depending on parameters

15

this reason, the two models seem to show qualitatively similar behavior under certain circumstances. While related, the full mechanisms are, nevertheless distinct. For example, the globally constrained Allen Cahn model does not support a stable homogeneous solution, unlike the model we discussed here.

In some of our numerical experiments (not shown), multiple peaks persisted for certain random initial data. We conjecture that these multiple peaks are metastable and that they eventually merge to form a single peak on a very long time scale. This prediction stems from the corresponding behavior of the globally constrained Allen Cahn model. A two dimensional generalization of the above model is expected to exhibit behavior analogous to that of the one dimensional model. In the initial phase, we expect to see expanding "islands" of the active form. This expansion will eventually come to a halt, corresponding to the phenomenon of wave-pinning explained in this paper. After this initial phase, the fronts will evolve to decrease mean curvature and the patches of the active forms will eventually merge to form a single patch. The predicted slow dynamics in this latter phase is analogous to that of the two-dimensional globally constrained Allen Cahn model. In two-dimensional exploratory simulations by Marée (personal communication), there is evidence to suggest that such is indeed the case. A more faithful physical model will be to have the active form diffuse on a 2D membrane and the inactive form diffuse in a 3D cytosol. We believe that such a model will also exhibit similar wave-pinning behavior, but this is yet to be confirmed. This and other mathematical issues will be dealt with in detail in future work.

Despite our belief that multiple peak solutions are metastable, the time scale on which they merge to form a single peak is too large to be biophysically relevant. If our mechanism is indeed an ingredient of the cell polarization machinery, the cell must possess other mechanisms to more quickly dissipate multiple peaks. Computational experiments with models that take into account the more detailed biochemical kinetics exhibit more rapid merging of multiple peaks, in line with biological observations. The key component here seems to be the presence of phosphoinositide pathways (46). We plan to clarify the precise role of this pathway in the context of the wave-pinning mechanism in a future study.

A   Appendix

A.1   Wave-pinning Model

To run the simulations of the wave-pinning model (Eqs. 5,3), we used parameter values described in the text. Time is in units of seconds. Concentration would typically be in some units of (quantity of molecules/length). We selected $b = 2.0$. The equation $f(a, b) = 0$ is then solved for a, yielding three values. The lowest of these, $a_-(b) = 0.2683312$, corresponds to the basal (low activation) rest state of the cell. Henceforth, for (a-c), we used the initial conditions $a = 0.2683312$, $b = 2.0$. This means that the total amount of material, $C = 10(a + b) = 22.6833$ is fixed and constant for all runs in Figure 2a-c.

A.2   Stimuli repertoire

The following set of stimuli were used to generate Figure 2 and comparable figures:

(a) **Transient localized stimulus:** We stimulated 10% of the domain, using

$$k_S^{\text{loc}} = \begin{cases} s(t)(1 + \cos \pi x), & 0 \le x \le 1, \\ 0 & \text{otherwise.} \end{cases}$$

where the time dependence was as follows:

$$s(t) = \begin{cases} \frac{S}{2} & 0 \le t \le t_1, \\ \frac{S}{4}\left(1 + \cos\left(\pi \frac{(t - t_1)}{(t_2 - t_1)}\right)\right), & t_1 \le t \le t_2, \\ 0, & \text{otherwise.} \end{cases}$$

$S = 0.05$, $t_1 = 20$, $t_2 = 25$ were used.

(b) **Transient graded stimulus:**

$$k_S^{\text{grad}} = s(t)(10 - x), \quad 0 \le x \le 10,$$

where

$$s(t) = \begin{cases} S, & 0 \le t \le t_1, \\ S\left(1 - \frac{t - t_1}{t_2 - t_1}\right), & t_1 \le t \le t_2, \\ 0, & \text{otherwise.} \end{cases} \tag{26}$$

$S = 0.07$, $t_1 = 20$, $t_2 = 25$ were used.

(c) **Reversal of graded stimulus:** We applied same stimulus k_S^{grad} as in (b) followed by

$$k_S^{\text{grad}} = s(t)x, \quad 0 \le x \le 10$$

where

$$s(t) = \begin{cases} S, & 200 \le t \le t_1, \\ S\left(1 - \frac{t - t_1}{t_2 - t_1}\right), & t_1 \le t \le t_2, \\ 0, & \text{otherwise.} \end{cases} \tag{27}$$

$S = 0.07$, $t_1 = 120$, $t_2 = 125$ were used.

(d) **Random initial conditions:**

Here $k_S \equiv 0$. We used nonuniform initial conditions of the form $a(x,0) = a_-(b_0) \cdot 2R$, $b(x,0) = b_0$ so that the noise has zero mean about the homogeneous steady state. The parameter values $a_-(b_0) = 0.2683312, b_0 = 2.0$, together with a uniformly distributed random number $R = UNIF(0,1)$ lead to some outcomes with polarization (as in Fig. 2d), some with long-lived multiple peaks, and some with decay back to homogenous distribution.

A.3 Simulations for Fig. 4

For Figure 4 we numerically solved the nondimensionalized system

$$\epsilon \frac{\partial a}{\partial t} = \epsilon^2 \frac{\partial^2 a}{\partial x^2} + f(a,b), \tag{28a}$$

$$\epsilon \frac{\partial b}{\partial t} = D \frac{\partial^2 b}{\partial x^2} - f(a,b). \tag{28b}$$

with $f(a,b) = a(0.8-a)(a-0.8-b)$ and $\epsilon = 0.01, D = 0.1$. The system is initialized with $b(0) = 1$ at the high steady state $(a(0) = 1.8)$ on $0 < x < 1/2$, and to the low steady state $(a(0) = 0)$ on $1/2 < x < 1$. It is integrated for 10 non-dimensional time units. Note that using typical parameter values for Rho GTPase $(L = 10\mu m, \ D_a = 0.1, D_b = 10\mu^2 s^{-1}, \ \gamma = 1 \ s^{-1})$ we obtain the small dimensionless quantity, $\epsilon = \sqrt{D_a/(\gamma L^2)} = 0.03$, and $D = D_b/(\gamma L^2) = 0.1$.

References

1. Meinhardt, H., and G. A, 1974. Application of a theory of biological pattern formation based on lateral inhibition. *J. Cell Sci.* 15:321–346.

2. Meinhardt, H., 1999. Orientation of chemotactic cells and growth cones: models and mechanisms. *J. Cell Sci.* 112:2867–2874.

3. Onsum, M., and C. V. Rao, 2007. A mathematical model for neutrophil gradient sensing and polarization. *PLoS Comput Biol.* 3:e36.

4. Levine, H., D. A. Kessler, and W.-J. Rappel, 2006. Directional sensing in eukaryotic chemotaxis: A balanced inactivation model. *Proc. Natl. Acad. Sci. USA* 103:9761–9766.

5. Gamba, A., A. de Candia, S. Di Talia, A. Coniglio, F. Bussolino, and G. Serini, 2005. Diffusion-limited phase separation in eukaryotic chemotaxis. *Proc. Natl. Acad. Sci. USA* 102:16927–16932.

6. Wong, K., O. Pertz, K. Hahn, and H. Bourne, 2006. Neutrophil polarization: Spatiotemporal dynamics of RhoA activity support a self-organizing mechanism. *Proc. Natl. Acad. Sci. USA* 103:3639–3644.

7. Janetopoulos, C., L. Ma, P. N. Devreotes, and P. A. Iglesias, 2004. Chemoattractant-induced phosphatidylinositol 3,4,5-trisphosphate accumulation is spatially amplified and adapts, independent of the actin cytoskeleton. *Proc. Natl. Acad. Sci. USA* 101:8951–8956.

8. Van Haastert, P., and P. Devreotes, 2004. Chemotaxis: signalling the way forward. *Nature Reviews Molecular Cell Biology* 6:626–634.

9. Iijima, M., Y. E. Huang, and P. Devreotes, 2002. Temporal and spatial regulation of chemotaxis. *Developmental Cell* 3:469–478.

10. Kimmel, A., and C. Parent, 2003. The signal to move: D-discoideum go orienteering. *Science* 300:1525–1527.

11. Meili, R., and R. Firtel, 2003. Two poles and a compass. *Cell* 114:153–156.

12. Etienne-Manneville, S., and A. Hall, 2002. Rho GTPases in cell biology. *Nature* 420:629–635.

13. Park, H.-O., and E. Bi, 2007. Central Roles of Small GTPases in the Development of Cell Polarity in Yeast and Beyond. *Microbiol. Mol. Biol. Rev.* 71:48–96.

14. Albrecht, E., and H. R. Petty, 1998. Cellular memory: Neutrophil orientation reverses during temporally decreasing chemoattractant concentrations. *PNAS* 95:5039–5044.

15. Killich, T., P. Plath, X. Wei, H. Bultmann, L. Rensing, and M. Vicker, 1993. The locomotion, shape and pseudopodial dynamics of unstimulated Dictyostelium cells are not random. *J Cell Sci* 106:1005–1013.

16. Andrew, N., and R. H. Insall, 2007. Chemotaxis in shallow gradients is mediated independently of PtdIns 3-kinase by biased choices between random protrusions. *Nature Cell Biology* 9:193–200.

17. Parent, C., and P. Devreotes, 1999. A cell's sense of direction. *Science* 284:765–770.

18. Levchenko, A., and P. Iglesias, 2002. Models of eukaryotic gradient sensing: Application to chemotaxis of amoebae and neutrophils. *Biophys. J.* 82:50–63.

19. Marée, A., A. Jilkine, A. Dawes, V. Grieneisen, and L. Edelstein-Keshet, 2006. Polarisation and movement of keratocytes: a multiscale modelling approach. *Bull. Math. Biol.* 68:1169–1211.

20. Jilkine, A., A. F. M. Marée, and L. Edelstein-Keshet, 2007. Mathematical model for spatial segregation of the Rho-family GTPases based on inhibitory crosstalk. *Bull. Math. Biol., April 25, Epub* .

21. Otsuji, M., S. Ishihara, C. Co, K. Kaibuchi, A. Mochizuki, and S. Kuroda, 2007. A Mass Conserved Reaction-Diffusion System Captures Properties of Cell Polarity. *PLoS Comput Biol.* 3(6):e108.

22. Giniger, E., 2002. How do Rho family GTPases direct axon growth and guidance? A proposal relating signaling pathways to growth cone mechanics. *Differentiation* 70:385–396.

23. Sakumura, Y., Y. Tsukada, N. Yamamoto, and S. Ishii, 2005. A molecular model for axon guidance based on cross talk between Rho GTPases. *Biophys. J.* 89:812–822.

24. Gierer, A., and M. H, 1972. A theory of biological pattern formation. *Kybernetik* 12:30–39.

25. Subramanian, K., and A. Narang, 2004. A mechanistic model for eukaryotic gradient sensing: Spontaneous and induced phosphoinositide polarization. *J. Theor. Biol.* 231:49–67.

26. Narang, A., 2006. Spontaneous polarization in eukaryotic gradient sensing: A mathematical model based on mutual inhibition of frontness and backness pathways. *J. Theor. Biol.* 240:538–553.

27. Krishnan, J., and P. A. Iglesias, 2007. Receptor-Mediated and Intrinsic Polarization and Their Interaction in Chemotaxing Cells. *Biophys. J.* 92:816–830.

28. Markevich, N. I., J. B. Hoek, and B. N. Kholodenko, 2004. Signaling switches and bistability arising from multisite phosphorylation in protein kinase cascades. *J. Cell Biol.* 164:353–359.

29. Markevich, N., M. Tsyganov, J. Hoek, and B. Kholodenko, 2006. Long-range signaling by phosphoprotein waves arising from bistability in protein kinase cascades. *Mol Syst Biol.* 2:61–69.

30. Ridley, A., 2001. Rho GTPases and cell migration. *J. Cell Sci.* 114:2713–2722.

31. Schmitz, A., E. Govek, B. Bottner, and van Aelst L, 2000. Rho GTPases: Signaling, migration, and invasion. *Experimental Cell Research* 261:1–12.

32. Bement, W. M., A. L. Miller, and G. von Dassow, 2006. Rho GTPase activity zones and transient contractile arrays. *BioEssays* 28:983–93.

33. Olofsson, B., 1999. Rho guanine dissociation inhibitors: pivotal molecules in cellular signalling. *Cell. Signal.* 11:545–554.

34. Zhang, B., and Y. Zheng, 1998. Regulation of RhoA GTP hydrolysis by the GTPase-activating proteins p190, p50RhoGAP, Bcr, and 3BP-1. *Biochem.* 37:5249–5257.

35. Postma, M., L. Bosgraaf, H. Loovers, and P. Van Haastert, 2004. Chemotaxis: signalling modules join hands at front and tail. *Embo Reports* 5:35–40.

36. Michaelson, D., J. Silletti, G. Murphy, P. Eustachio, M. Rush, and M. Philips, 2001. Differential localization of Rho GTPases in live cells: Regulation by hypervariable regions and RhoGDI binding. *J. Cell Biol.* 152:111–126.

37. Bement, W. M., H. A. Benink, and G. von Dassow, 2005. A microtubule-dependent zone of active RhoA during cleavage plane specification. *J Cell Biol.* 170:91–101.

38. Pertz, O., L. Hodgson, R. Klemke, and K. Hahn, 2006. Spatiotemporal dynamics of RhoA activity in migrating cells. *Nature* 440:1069–1072.

39. Charest, P., and R. Firtel, 2007. Big roles for small GTPases in the control of directed cell movement. *Biochem J* 401:377–90.

40. Krishnan, J., and P. Iglesias, 2004. A modeling framework describing the enzyme regulation of membrane lipids underlying gradient perception in Dictyostelium cells. *J. Theor. Biol.* 229:85–99.

41. Haugh, J., and I. Schneider, 2004. Spatial analysis of 3 ' phosphoinositide signaling in living fibroblasts: I. Uniform stimulation model and bounds on dimensionless groups. *Biophys. J.* 86:589–598.

42. Maly, I., H. Wiley, and D. Lauffenburger, 2004. Self-organization of polarized cell signaling via autocrine circuits: Computational model analysis. *Biophys. J.* 86:10–22.

43. Skupsky, R., W. Losert, and R. Nossal, 2005. Distinguishing modes of eukaryotic gradient sensing. *Biophys. J.* 89:2806–2823.

44. Krishnan, J., and P. Iglesias, 2004. Uncovering directional sensing: where are we headed? *Systems Biology* 1:54–61.

45. Devreotes, P., and C. Janetopoulos, 2003. Eukaryotic chemotaxis: Distinctions between directional sensing and polarization. *J. Biol. Chem.* 278:20445–20448.

46. Dawes, A., and L. Edelstein-Keshet, 2007. Phosphoinositides and Rho proteins spatially regulate actin polymerization to initiate and maintain directed movement in a 1D model of a motile cell. *Biophys J* 92:1–25.

47. Ma, L., C. Janetopoulos, L. Yang, P. Devreotes, and P. Iglesias, 2004. Two complementary, local excitation, global inhibition mechanisms acting in parallel can explain the chemoattractant-induced regulation of PI(3,4,5)P-3 response in Dictyostelium cells. *Biophys. J.* 87:3764–3774.

48. Meinhardt, H., 1982. Models of Biological Pattern Formation. Academic, New York.

49. Murray, J., 1993. Mathematical Biology, Second Edition. Springer.

50. Amari, S., 1977. Dynamics of pattern formation in lateral-inhibition type neural fields. *Biological Cybernetics* 27:77–87.

51. Cross, M. C., and P. C. Hohenberg, 1993. Pattern formation outside of equilibrium. *Rev. Mod. Phys.* 65:851.

52. Meinhardt, H., and P. A. J. de Boer, 2001. Pattern formation in Escherichia coli: A model for the pole-to-pole oscillations of Min proteins and the localization of the division site. *Proceedings of the National Academy of Sciences* 98:14202–14207.

53. Ozbudak, E. M., A. Becskei, and van Oudenaarden A, 2005. A system of counteracting feedback loops regulates Cdc42p activity during spontaneous cell polarization. *Dev. Cell* 9:565–71.

54. Marco, E., R. Wedlich-Soldner, R. Li, S. Altschuler, and W. L.F., 2007. Endocytosis optimizes the dynamic localization of membrane proteins that regulate cortical polarity. *Cell* 129:411–22.

55. Sako, Y., K. Hibino, T. Miyauchi, Y. Miyamoto, M. Ueda, and T. Yanagida, 2000. Single-molecule imaging of signaling molecules in living cells. *Single Mol.* 1:159–163.

56. Janetopoulos, C., J. Borleis, F. Vazquez, M. Iijima, and P. Devreotes, 2005. Temporal and spatial regulation of phosphoinositide signaling mediates cytokinesis. *Dev. Cell* 8:467–477.

57. Keener, J., and J. Sneyd, 1998. Mathematical Physiology. Springer.

58. Kessler, D. A., and H. Levine, 1990. Stability of traveling waves in the Belousov-Zhabotinskii reaction. *Phys. Rev. A* 41:5418–5430.

59. Kutscher, B., P. Devreotes, and P. Iglesias, 2004. Local Excitation, Global Inhibition Mechanism for Gradient Sensing: An Interactive Applet. *Science's STKE* 219:pI3.

60. Meinhardt, H., 2003. The Algorithmic Beauty of Sea Shells, 3rd Ed. Springer, Heidelberg, New York.

61. Iglesias, P. A., and A. Levchenko, 2002. Modeling the cell's guidance system. *Sci. STKE* 2002:RE12.

62. Nicolis, G., and I. Prigogine, 1977. elf-organization in nonequilibrium systems. Wiley, New York.

63. Weiner, O., W. Marganski, L. Wu, S. Altschuler, and M. Kirschner, 2007. An Actin-Based Wave Generator Organizes Cell Motility. *PLoS Biol.* 5:e221.

64. Lin, Q., W. Yang, D. Baird, Q. Feng, and R. A. Cerione, 2006. Identification of a DOCK180-related Guanine Nucleotide Exchange Factor That Is Capable of Mediating a Positive Feedback Activation of Cdc42. *J. Biol. Chem.* 281:35253–35262.

65. DerMardirossian, C., A. Schnelzer, and G. M. Bokoch, 2004. Phosphorylation of RhoGDI by Pak1 Mediates Dissociation of Rac GTPase. *Molecular Cell* 15:117–127.

66. DerMardirossian, C., G. Rocklin, J.-Y. Seo, and G. M. Bokoch, 2006. Phosphorylation of RhoGDI by Src Regulates Rho GTPase Binding and Cytosol-Membrane Cycling. *Mol. Biol. Cell* 17:4760–4768.

67. Irazoqui, J., A. Gladfelter, and D. Lew, 2003. Scaffold-mediated symmetry breaking by Cdc42p. *Nature Cell Biol.* 5:1062–70.

68. Xu, J., F. Wang, A. Van Keymeulen, P. Herzmark, A. Straight, K. Kelly, Y. Takuwa, N. Sugimoto, T. Mitchison, and H. Bourne, 2003. Divergent signals and cytoskeletal assemblies regulate self-organizing polarity in neutrophils. *Cell* 114:201–214.

69. Wylie, J. J., and M. R. M., 2006. Traveling waves in coupled reaction-diffusion models with degenerate sources. *Phys. Rev. E* 74:021909.

70. Sepulchre, J.-A., and V. I. Krinsky, 2000. Bistable reaction-diffusion systems can have robust zero-velocity fronts. *Chaos* 10:826–833.

71. Kramer, L., G. Gottwald, V. Krinsky, A. Pumir, and V. V. Barelko, 2000. Persistence of zero velocity fronts in reaction diffusion systems. *Chaos* 10:731–737.

72. Rubinstein, J., and P. Sternberg, 1992. Nonlocal reaction–diffusion equations and nucleation. *IMA Journal of Applied Mathematics* 48:249.

73. Meerson, B., and P. Sasorov, 1996. Domain stability, competition, growth, and selection in globally constrained bistable systems. *Physical Review E* 53:3491–3494.

74. Ward, M., 1996. Metastable Bubble Solutions for the Allen-Cahn Equation with Mass Conservation. *SIAM Journal on Applied Mathematics* 56:1247–1279.

Figure Legends

Figure 1

(a) A schematic diagram of the membrane translocation cycle of a typical Rho family GTPase and its approximation by the $A - B$ reaction-diffusion system. The inactive cytosolic form diffuses much faster than the active membrane-bound form and is approximately uniformly distributed. (b) Schematic diagram, showing the assumed 1D spatial geometry of the cell in a side view. The axis $0 < x < L$ represents a cell diameter (length $L \approx 10\mu$m) with no-flux boundary conditions. Membrane thickness is exaggerated for visibility. Active/inactive Rho proteins are represented by solid/open disks, and assumed to diffuse along the axis of the cell in both membrane and cytosol. Polarization corresponds to concentration of the active form in the membrane at the nascent cell front. Typical profiles of active (a) and inactive (b) proteins, and the position of the sharp front, x_f, is shown in the lower panel.
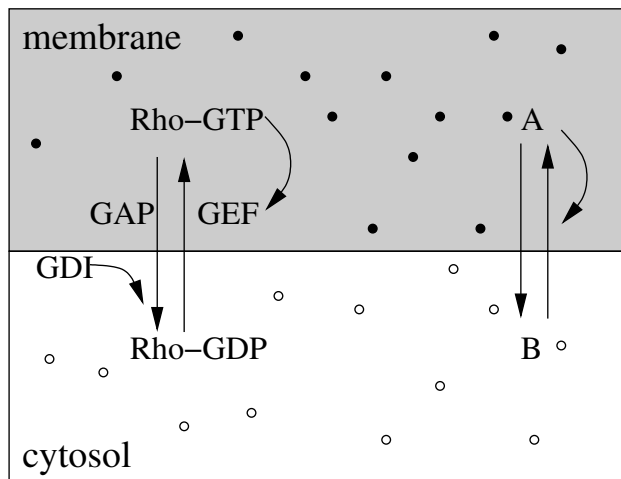
Figure 2

Wave-pinning: Polarization behaviour in response to four distinct stimuli and/or initial conditions computed numerically for the model system given by Eqs. 5 with the reaction term of Eq. 3 and parameter values given in the text. Initial conditions (lowest line/curve), transient ($t = 20$s), and asymptotic behaviour ($t = 200$s) are shown by solid lines. The final position of the wavefront (at $t = 200$) does not depend on the stimuli (dotted lines), but only on the total amount of material, which is the same in all cases. Detailed forms of stimuli are given in the Appendix. (a) A localized stimulus k_S^{loc}, of amplitude of 0.05 (enlarged for clarity) is applied at $t = 0$ for 20s. (b) A graded stimulus of amplitude 0.01, k_S^{grad} is applied at $t = 0$ for 20s. (c) As in (b), but a graded stimulus of amplitude 0.02 for 20s at $t = 0$ is followed, at $t = 200$, by a similar graded stimulus of reverse orientation for 20s (k_S^{resp}). The first stimulus defines one polarization (at $t = 200$), but the second stimulus causes the system to reverse polarity (curve labeled $t = 400$). (d) Large amplitude noise, superimposed on the homogeneous initial conditions, with no additional stimulus (see Appendix) also leads to polarization.
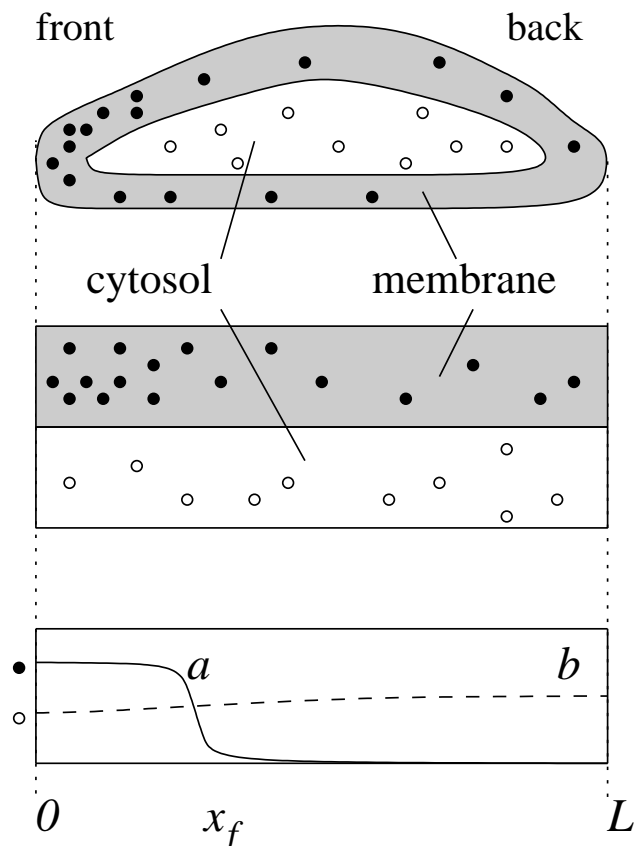
Figure 3

A diagram schematically explaining wave-pinning behavior. The left column plots the concentrations of a and b versus position x whereas the right column plots the reaction terms (LHS and RHS of Eq. 4) as functions of a. At the beginning, the value of the integral $I(b)$ (numerator of Eq. 10 and difference of shaded areas) is positive, and the wave front moves to the right (top figure). As the wave front sweeps across the domain, b and hence $I(b)$ decreases, and the wave decelerates (middle). The wave eventually comes to a halt when shaded areas are equal ($I(b) = 0$, bottom).

Figure 4

Initial conditions $a(0), b(0)$ and eventual solutions $a(10), b(10)$ to a nondimensionalized variant of Eqs. 5 with the cubic kinetics function of Eq. 13 are shown in (a) for asymptotically large D_a/D_b. The evolution of the steepest point x_f through time and the solution of Eq. 17 is shown in (b). See Appendix for further details.
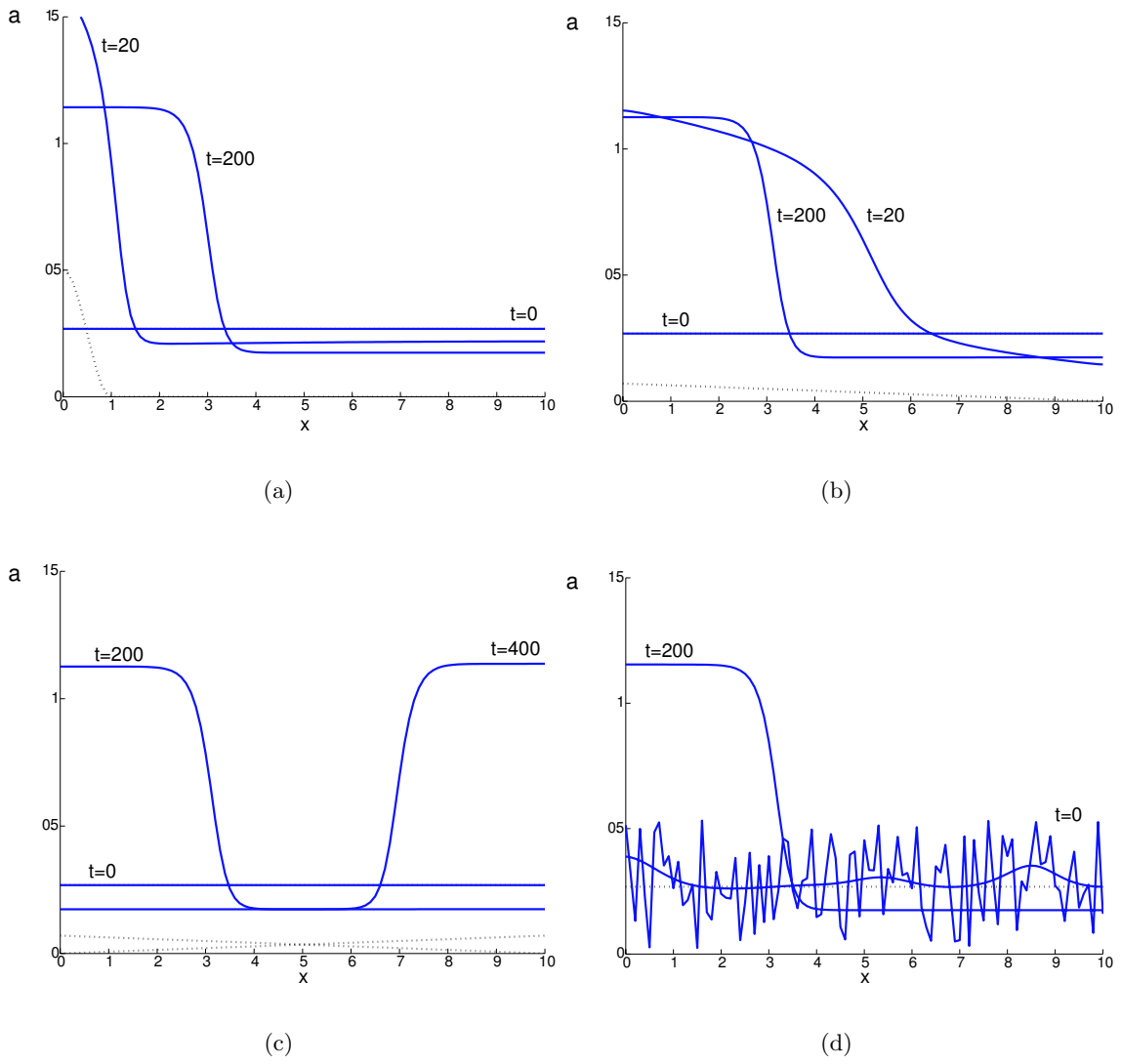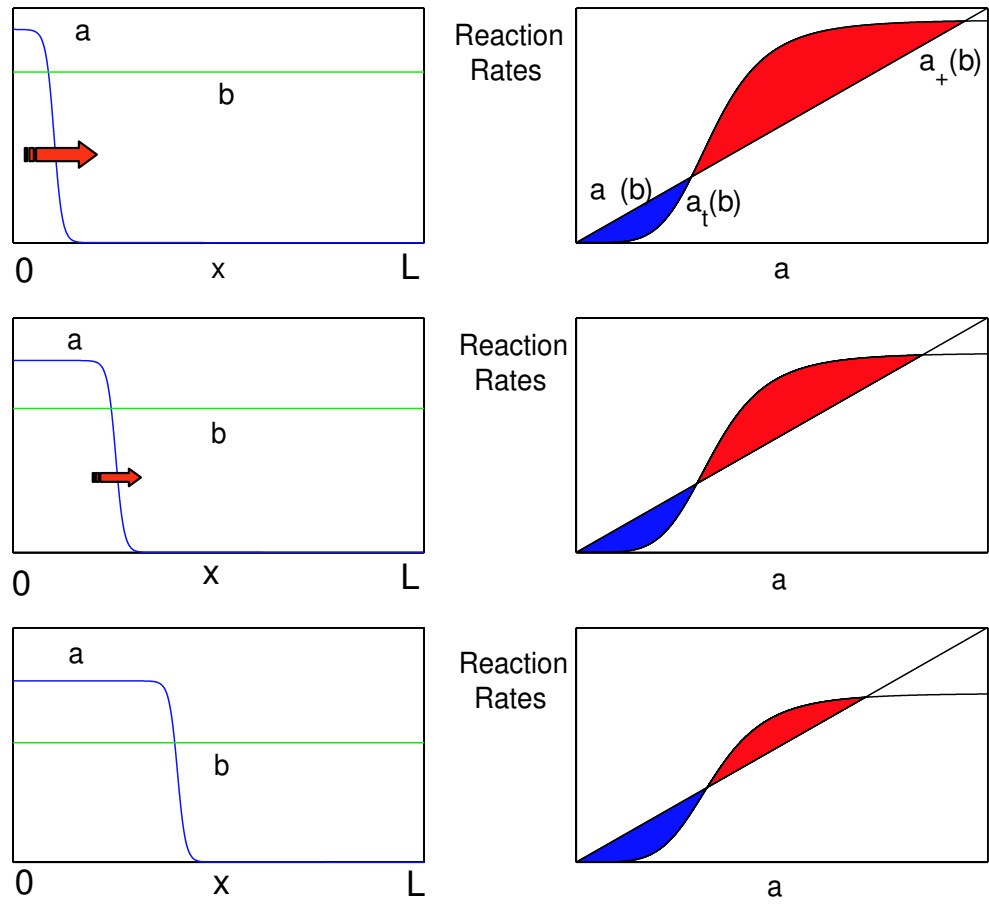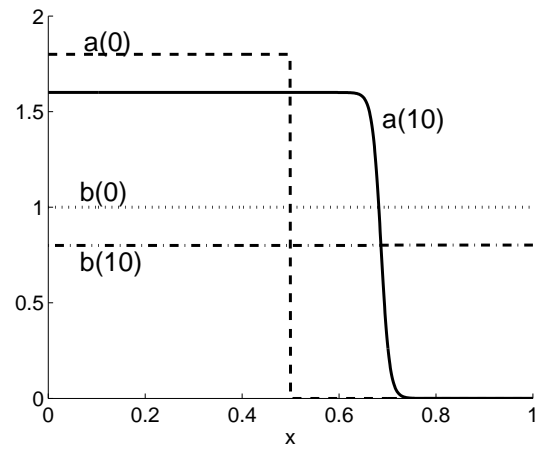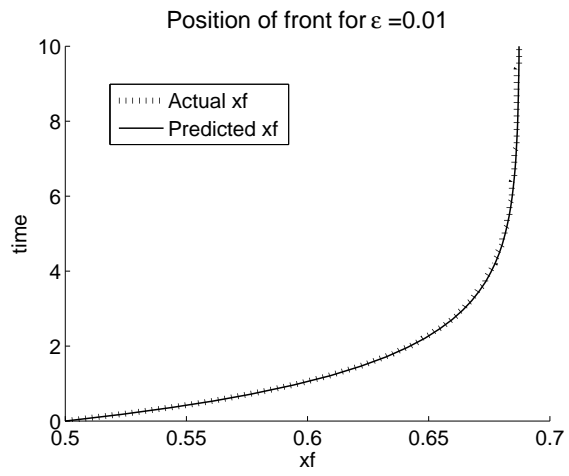
(a)

(b)

Figure 1:

Figure 2:

(a)

Figure 3:

(a)

(b)

Figure 4: